

On the Emerging Potential of Quantum Annealing Hardware for Combinatorial Optimization

Byron Tasseff

Los Alamos National Laboratory, Los Alamos, NM 87545

Tameem Albash

University of New Mexico, Albuquerque, NM 87131

Zachary Morrell, Marc Vuffray, Andrey Y. Lokhov, Sidhant Misra, Carleton Coffrin*
Los Alamos National Laboratory, Los Alamos, NM 87545

Abstract

Over the past decade, the usefulness of quantum annealing hardware for combinatorial optimization has been the subject of much debate. Thus far, experimental benchmarking studies have indicated that quantum annealing hardware does not provide an irrefutable performance gain over state-of-the-art optimization methods. However, as this hardware continues to evolve, each new iteration brings improved performance and warrants further benchmarking. To that end, this work conducts an optimization performance assessment of D-Wave Systems' most recent *Advantage Performance Update* computer, which can natively solve sparse unconstrained quadratic optimization problems with over 5,000 binary decision variables and 40,000 quadratic terms. We demonstrate that classes of contrived problems exist where this quantum annealer can provide run time benefits over a collection of established classical solution methods that represent the current state-of-the-art for benchmarking quantum annealing hardware. Although this work *does not* present strong evidence of an irrefutable performance benefit for this emerging optimization technology, it does exhibit encouraging progress, signaling the potential impacts on practical optimization tasks in the future.

1 Introduction

In the 1990s, an optimization algorithm called quantum annealing (QA) was proposed with the aim of providing a fast heuristic for solving combinatorial optimization problems [44, 68, 26, 23, 71]. At a high level, QA is an analog quantum algorithm that leverages the non-classical properties of quantum systems and continuous time evolution to minimize a discrete function. *Annealing* is the process that steers the dynamics of the quantum system into an a priori unknown minimizing variable assignment of that function. Under suitable conditions, theoretical results have shown that QA can arrive at a global optimum of the desired function [10, 45, 40]. These results have motivated the study of using this algorithm for combinatorial optimization over the past thirty years.

Due to the computational difficulty of simulating quantum systems [25], the study of QA remained a theoretical pursuit until 2011, when D-Wave Systems produced a quantum hardware implementation of the QA algorithm [6, 43, 33, 42]. This represented the first time that QA could be studied on optimization problems with more than a few dozen decision variables and spurred significant interest in developing a better understanding of the QA computing model [41, 35, 12].

The release of D-Wave Systems' QA hardware platform also generated expectations that this new technology would quickly outperform state-of-the-art classical methods for solving well-suited combinatorial

*corresponding author, cjc@lanl.gov

optimization problems [23, 22, 71]. The initial interest from the operations research community was significant. However, through careful comparison with both complete search solvers [59, 67, 18] and specialized heuristics [73, 8, 72, 56, 55, 70, 36, 2], it was determined that the available QA hardware was a far cry from state-of-the-art optimization methods. These results tempered the excitement around the QA computing model and reduced interest from the operations research community. Since the waning of the initial excitement around QA, QA hardware has steadily improved and now features better noise characteristics [78, 79, 47] and quantum computers that can solve optimization problems more than fifty times larger than what was possible in 2013 [58].

Since 2017, we have been using the benchmarking practices of operations research to track the performance of QA hardware platforms and compare the results with established optimization algorithms [11, 66]. In previous studies of this type, this benchmarking approach ruled out any potential performance benefit for using available QA hardware platforms in hybrid optimization algorithms and practical applications, as established algorithms outperformed or were competitive with the QA hardware in both solution quality and computation time. However, in this work, we report that with the release of D-Wave Systems’ most recent *Advantage Performance Update* computer in 2021, our benchmarking approach can no longer rule out a potential run time performance benefit for this hardware. In particular, we show that there exist classes of combinatorial optimization problems where this QA hardware finds high-quality solutions around fifty times faster than a wide range of heuristic algorithms under best-case QA communication overheads and around fifteen times faster under real-world QA communication overheads. This work thus provides compelling evidence that quantum computing technology has the potential for accelerating *certain* combinatorial optimization tasks. This represents an important and necessary first condition for demonstrating that QA hardware can have an impact on solving practical optimization problems.

Although this work demonstrates encouraging results for the QA computing model, we also emphasize that it *does not* provide evidence of a fundamental or irrefutable performance benefit for this technology. Indeed, it is quite possible that dramatically different heuristic algorithms [21, 63] or alternative hardware technologies [60, 32, 57, 53] can reduce the run time performance benefits observed in this work. We look forward to and encourage ongoing research into benchmarking the QA computing model, as closing the performance gap presented in this work would provide significant algorithmic insights into heuristic optimization methods, benefiting a variety of practical optimization tasks.

This work begins with a brief introduction to the types of combinatorial optimization problems that can be solved with QA hardware and the established benchmarking methodology in Section 2. It then presents a summary of the key outcomes from a large-scale benchmarking study in Section 3, which required hundreds of hours of compute time. In Section 4, the paper concludes with some discussion of the limitations of our results and future opportunities for QA hardware in combinatorial optimization. Additional details regarding the experimental design, as well as further analyses of computational results, are provided in the appendices.

2 Quantum Annealing for Combinatorial Optimization

Available QA hardware is designed to perform optimization of a class of problems known as *Ising models*, which have historically been used as fundamental modeling tools in statistical mechanics [28]. Ising models are characterized by the following quadratic *energy* (or objective) function of $\mathcal{N} = \{1, 2, \dots, n\}$ discrete *spin* variables, $\sigma_i \in \{-1, 1\}$, $\forall i \in \mathcal{N}$:

$$E(\sigma) = \sum_{(i,j) \in \mathcal{E}} J_{ij} \sigma_i \sigma_j + \sum_{i \in \mathcal{N}} h_i \sigma_i, \quad (1)$$

where the parameters, J_{ij} and h_i , define the quadratic and linear coefficients of this function, respectively. The edge set, $\mathcal{E} \subseteq \mathcal{N} \times \mathcal{N}$, is used to encode a specific sparsity pattern in the Ising model, which is determined by the physical system being considered. The optimization task of interest is to find the lowest energy configuration(s) of the Ising model, i.e.,

$$\begin{aligned} & \underset{\sigma}{\text{minimize}} && E(\sigma) \\ & \text{subject to} && \sigma_i \in \{-1, 1\}, \forall i \in \mathcal{N}. \end{aligned} \quad (2)$$

At first glance, the lack of constraints and limited types of variables make this optimization task appear distant from real-world applications. However, the optimization literature on *quadratic unconstrained binary*

optimization (QUBO), which is equivalent to minimization of an Ising model’s energy function, indicates how this model can encode a wide range of practical optimization problems [51, 54].

2.1 Foundations of Quantum Annealing

The central idea of QA is to leverage the properties of quantum systems to minimize discrete-valued functions, e.g., finding optimal solutions to Problem (2). The mathematics of QA is comprised of two key elements: (i) leveraging quantum states to lift the minimization problem into an exponentially larger space and (ii) slowly interpolating (i.e., annealing) between an initial easy problem and the target problem to find high-quality solutions to the target problem. The quantum lifting begins by introducing, for each spin, $\sigma_i \in \{-1, 1\}$, a $2^{|\mathcal{N}|} \times 2^{|\mathcal{N}|}$ dimensional matrix, $\hat{\sigma}_i$, expressible as a Kronecker product of $|\mathcal{N}|$ 2×2 matrices,

$$\hat{\sigma}_i = \underbrace{\begin{pmatrix} 1 & 0 \\ 0 & 1 \end{pmatrix} \otimes \cdots \otimes \begin{pmatrix} 1 & 0 \\ 0 & 1 \end{pmatrix}}_{1 \text{ to } i-1} \otimes \underbrace{\begin{pmatrix} 1 & 0 \\ 0 & -1 \end{pmatrix}}_i \otimes \underbrace{\begin{pmatrix} 1 & 0 \\ 0 & 1 \end{pmatrix} \otimes \cdots \otimes \begin{pmatrix} 1 & 0 \\ 0 & 1 \end{pmatrix}}_{i+1 \text{ to } |\mathcal{N}|}. \quad (3)$$

In this lifted representation, the value of a spin, σ_i , is identified with the two possible eigenvalues, 1 and -1 , of the matrix $\hat{\sigma}_i$. The quantum counterpart of the energy function defined in Equation (1) is the $2^{|\mathcal{N}|} \times 2^{|\mathcal{N}|}$ matrix obtained by substituting spins, σ_i , with the $\hat{\sigma}_i$ matrices, defined in Equation (3), within the algebraic expression for the energy. That is,

$$\hat{E} = \sum_{(i,j) \in \mathcal{E}} J_{ij} \hat{\sigma}_i \hat{\sigma}_j + \sum_{i \in \mathcal{N}} h_i \hat{\sigma}_i. \quad (4)$$

Notice that the eigenvalues of the matrix \hat{E} are the $2^{|\mathcal{N}|}$ possible energies obtained by evaluating $E(\sigma)$ from Equation (1) for all possible configurations of spins. This implies that finding the minimum eigenvalue of \hat{E} is equivalent to solving Problem (2). This lifting is clearly impractical in the classical computing context, as it transforms a minimization problem over $2^{|\mathcal{N}|}$ configurations into computing the minimum eigenvalue of a $2^{|\mathcal{N}|} \times 2^{|\mathcal{N}|}$ matrix. The key motivation for the QA computational approach is that it is possible to model \hat{E} with only $|\mathcal{N}|$ quantum bits (qubits), so it is feasible to compute over this exponentially large matrix.

The annealing process in QA provides a method for steering a quantum system into the a priori unknown eigenvector that minimizes Equation (4) [44, 24]. First, the system is initialized at an a priori *known* minimizing eigenvector of a simple (“easy”) energy matrix, \hat{E}_0 . After the system has been initialized, the energy matrix is interpolated from the easy problem to the target problem slowly over time. Specifically, the energy matrix at a point during the anneal is $\hat{E}_a(\Gamma) = (1 - \Gamma)\hat{E}_0 + \Gamma\hat{E}$, with Γ varying from zero to one. The annealing time is the physical time taken by the system to evolve from $\Gamma = 0$ to $\Gamma = 1$. When the anneal is complete ($\Gamma = 1$), the interactions in the quantum system are described by the target energy matrix. For suitable starting energy matrices, \hat{E}_0 , and a sufficiently slow annealing time, the adiabatic theorem demonstrates that a quantum system remains at the minimal eigenvector of the interpolating matrix, $\hat{E}_a(\Gamma)$ [10, 45, 40], and therefore achieves the minimum energy of the target problem.

2.2 Quantum Annealing Hardware

The computers developed by D-Wave Systems realize the QA computational model in hardware with more than 5,000 qubits. However, the engineering challenges of building real-world quantum computers are significant and have an impact on the previously discussed theoretical model of QA. In particular, QA hardware is an open quantum system, meaning that it is affected by environmental noise and decoherence. The coefficients in Equation (1) are constrained to the ranges, $-4 \leq h_i \leq 4$, $-1 \leq J_{ij} \leq 1$, and nonzero J_{ij} values are restricted to a specific sparse lattice structure (i.e., $\mathcal{E}^H \subseteq \mathcal{E}$), which is determined by the hardware’s implementation. (See Appendix A for details.) The D-Wave hardware documentation also highlights five sources of deviation from ideal system operations called *integrated control errors*, which include background susceptibility, flux noise, digital-to-analog conversion quantization, input/output system effects, and variable scale across qubits [14]. These implementation details impact the performance of QA hardware [64]. Consequently, QA hardware often does not find globally optimal solutions but instead finds near-optimal solutions, e.g., within 1% of global optimality [11]. All of these deviations from the ideal QA setting present

notable challenges for encoding and benchmarking combinatorial optimization problems with available QA hardware platforms.

2.3 Benchmarking Quantum Annealing Hardware

Due to the challenges associated with mapping established optimization test cases to specific QA hardware [11], the QA benchmarking community has adopted the practice of building instance generation algorithms that are tailored to specific quantum processing units (QPUs) [48, 36, 49, 19, 2, 66]. The majority of the proposed problem generation algorithms build Ising model instances that are defined over a specific QPU’s hardware graph, i.e., $(\mathcal{N}, \mathcal{E}^H)$, or subsets of this graph, which are typically referred to as *hardware-native* problems.

In this work, we build upon an earlier class of hardware-native instances termed *corrupted biased ferromagnets*, or CBFMs, as proposed by [66]. Given the QPU graph, $(\mathcal{N}, \mathcal{E}^H)$, the CBFM model adopts the following distributions for hardware-native instances:

$$\begin{aligned} P(J_{ij} = 0) = 0, P(J_{ij} = -1) = 0.625, P(J_{ij} = 0.2) = 0.375, \forall (i, j) \in \mathcal{E}^H \\ P(h_i = 0) = 0.97, P(h_i = -1) = 0.02, P(h_i = 1) = 0.01, \forall i \in \mathcal{N}. \end{aligned} \tag{CBFM}$$

Benchmarking these instances on the previous generation of D-Wave’s QPU architecture (i.e., the 2000Q platform using the CHIMERA hardware graph) showed promising performance against state-of-the-art classical alternatives, although a clear wall-clock run time benefit was not achieved [66].

In this work, we design a variant of the CBFM problem class called CBFM-P, which is tailored to D-Wave’s new *Advantage* QPU platform. The parameter distributions are

$$\begin{aligned} P(J_{ij} = 0) = 0.35, P(J_{ij} = -1) = 0.10, P(J_{ij} = 1) = 0.55, \forall (i, j) \in \mathcal{E}^H \\ P(h_i = 0) = 0.15, P(h_i = -1) = 0.85, P(h_i = 1) = 0, \forall i \in \mathcal{N}. \end{aligned} \tag{CBFM-P}$$

The CBFM-P parameters differ from CBFM, as the new Advantage QPU architecture features a different and denser hardware graph called PEGASUS, whose topology is detailed in Appendix A. These parameters were discovered using a metaheuristic approach that explored different combinations of the twelve parameters in this model and sought to maximize the problem’s difficulty. In each evaluation of the metaheuristic, a combination of parameters was selected, one random instance was generated following this parameterization, and a variety of classical solution methods were executed on the instance. The instance difficulty was determined by comparing the lower and upper bounds of solutions found by these classical solution methods. Although this approach is naive, we found that it was sufficient for the objectives of this study. We expect that there exist classes of more challenging hardware-native instances on the PEGASUS graph, but identifying these classes is left for future work.

3 Optimization Performance Analysis

In this section, we compare the performance of the D-Wave Advantage QPU and a variety of classical algorithms for optimization of CBFM-P Ising models. Specifically, we consider the following established classical algorithms:

- A greedy algorithm based on steepest coordinate descent (SCD) [66];
- An integer quadratic programming (IQP) model formulation solved using the commercial mathematical programming solver GUROBI [7];
- Simulated annealing (SA) [76, 16];
- A spin-vector Monte Carlo (SVMC) algorithm, which was proposed to approximate the behavior of QA [74];
- Parallel tempering with iso-energetic clustering moves (PT-ICM) [80].

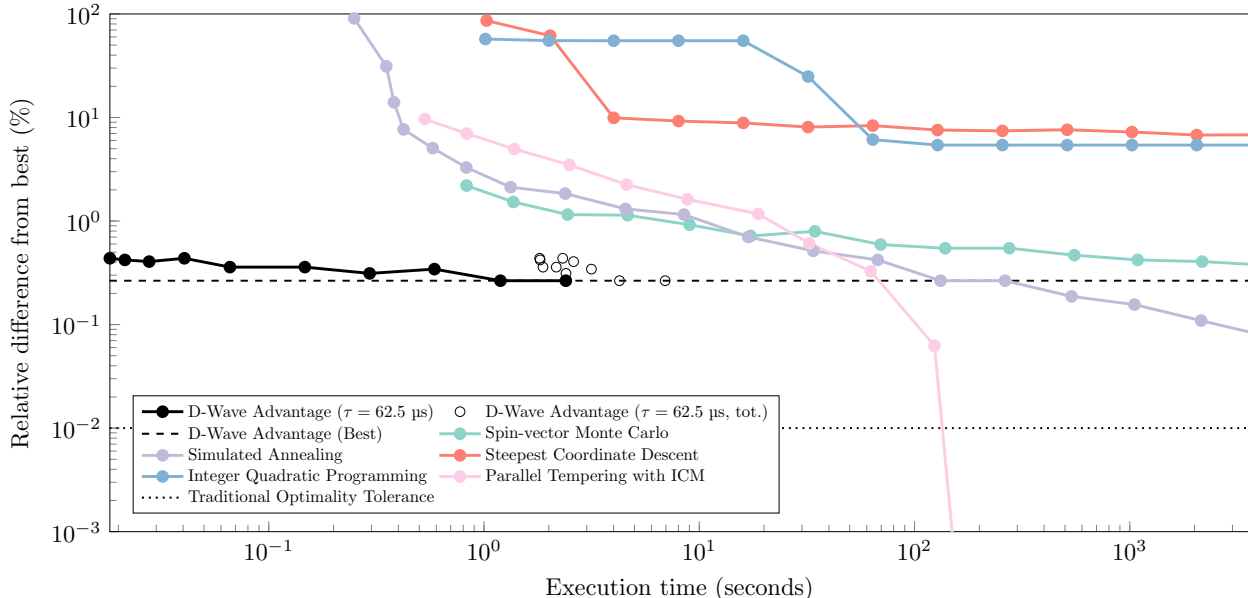


Figure 1: Evaluation of solution quality for a characteristic example of the CBFM-P instance class with 5,387 decision variables. Although the `Advantage_system4.1` QPU does not find the best-known solution, it consistently and quickly finds solutions within 0.5% of the best-known solution. Here, the dashed line corresponds to the achieved solution quality from QA when using 2,560 anneal-read cycles, as used in subsequent analyses. For comparison, the dotted line corresponds to a traditional optimization tolerance of 0.01%, as typically used by mathematical programming solvers as a termination criterion.

SCD and IQP are general optimization approaches, intended to serve as strawman comparisons to understand solution quality, while SA, SVMC, and PT-ICM reflect high-performance classical competitors, which provide different tradeoffs in run time and solution quality. Details of these methods and others that were considered are discussed in Appendix B. All of these classical optimization algorithms were executed on a system with two Intel Xeon E5-2695 v4 processors, each with 18 cores at 2.10 GHz, and 125 GB of memory. The parameterizations used by each algorithm in this work are also detailed in Appendix B.

For the QA hardware comparison, we use the `Advantage_system4.1` QPU accessed through D-Wave Systems’ LEAP cloud platform. The largest system we consider features $|\mathcal{N}| = 5,387$ discrete variables and $|\mathcal{E}^H| = 25,324$ quadratic coefficients in the PEGASUS topology. Solving a hardware-native optimization problem on this platform consists of (i) programming an Ising model, (ii) repeating the annealing and read-out process a number of times, and (iii) returning the highest quality solution found over all replicates. In this analysis, we hold the annealing time constant at 62.5 μs , which is justified in Appendix C. The number of anneal-read cycles are varied between 10 and 5,120 to produce different total run times. We also leverage the *spin reversal transforms* feature, provided by the LEAP platform, after every 100 anneal-read cycles to mitigate the undesirable impacts of the aforementioned integrated control errors. For each Ising instance, this protocol typically requires less than two seconds of QPU compute time and less than 10 seconds of total wall-clock time.

3.1 A Characteristic Example

Here, we present an evaluation of the above optimization techniques on a characteristic problem instance of the largest CBFM-P Ising models that we considered on the `Advantage_system4.1` QPU, with 5,387 variables.¹ For each solution technique, parameters that control the execution time of the algorithm (e.g., the number of sweeps in SA or the wall-clock time limit of the IQP method) were varied to understand their effects on solution quality. These parameters are detailed in Appendix B. All other parameters remained

¹An evaluation over 50 CBFM-P instances in Appendix D indicates this example is not an outlier.

fixed.

Benchmarking results for the CBFM-P instance “16” are shown in Figure 1. Here, the horizontal axis measures the execution time of each algorithm, where each point indicates the best solution at the end of an independent algorithm execution with some set termination criterion. The vertical axis measures the solution quality as the relative difference from the best-known solution. Specifically, each solution’s relative difference is computed as

$$\% \text{ Relative Difference} = 100\% \left(\frac{|\bar{E} - E^*|}{|E^*|} \right), \tag{5}$$

where E^* is the best-known objective value, i.e., the energy of Equation (1) for the best-known solution, and \bar{E} is the objective value obtained for a specific solver and execution time.

In Figure 1, we first observe that the QPU (i.e., the solid black line) is shown to find high-quality, but not optimal, solutions at very fast timescales (between 0.01 and 2.40 seconds), with relative quality differences between 0.2% and 0.5% of the best-known solution. Note that each execution time comprising the solid black line reflects a setting where the classical computer is colocated with and has exclusive access to the QPU. In practice, QPU access is managed by D-Wave’s remote cloud service, LEAP, which has overheads in both communication and job scheduling. These solve times are reflected by the open points in Figure 1, which add between one and five seconds of overhead to the total idealized solve times. Impressively, even accounting for these significant overheads, the QPU is still able to obtain high-quality solutions well before all other classical methods that are considered.

Although the `Advantage.system4.1` QPU is capable of quickly obtaining high-quality solutions in short amounts of time, it appears to reach a solution quality limit around 0.2%. This relative difference is over an order of magnitude larger than the standard termination criterion used by mathematical programming solvers, i.e., an optimality gap of 0.01% or less, delineated by the dotted line in Figure 1. To facilitate a comparison of the run time performance gained by the `Advantage.system4.1` QPU, we thus propose a measurement that evaluates the ability of classical algorithms to *match* the solution quality found by the QPU after 2,560 anneal-read cycles. The measurement we use is similar to determining the intersection with the dashed line in Figure 1, albeit on a linear instead of logarithmic scale.

In this instance example, the best solution obtained by the QPU after 2,560 anneal-read cycles is discovered after around 1.2 seconds when neglecting overheads and 4.3 seconds when including overheads. Most solution techniques (i.e., SVMC, IQP, and SCD) do not reach this solution quality after one hour of computation. Simulated annealing matches this quality after around 132 seconds and, linearly interpolating between the two nearest points before and after the intersection, PT-ICM is estimated to match this quality after around 77 seconds. Thus, the *best-case* performance of the QPU in this experiment, which assumes colocation with and direct access to the QPU, provides a 64 times improvement in run time, from 77 seconds with PT-ICM to 1.2 seconds. A similar comparison using the wall-clock run time yields an improvement of around 18 times. That is, even when including the overhead of communicating with D-Wave’s LEAP cloud service, the QPU is capable of providing a high-quality solution over an order of magnitude faster than all tested classical methods.

3.2 Problem Scaling Run Time Trends

In this subsection, we investigate how the run time performance of the QPU is impacted by the size of the problem that is considered. Unlike the previous section, here, we consider solution statistics that are *aggregated* over 50 distinct CBFM-P instances per problem size. Similar to the run time ratios discussed in Section 3.1, we estimate the amount of time required for the classical algorithms to match, on average, the solution quality reported by the QPU using an annealing time of 62.5 μ s and 2,560 anneal-read cycles. This experiment is performed for PEGASUS lattice sizes ranging from two to sixteen, yielding problems with 40 to 5,387 decision variables. For each instance, if a classical algorithm exactly matches the best solution (objective) found by the QPU, this *time-to-match* measurement is the earliest solve time at which that solution is obtained. If a classical algorithm finds a solution that does not strictly match but is *better* than the solution found using the QPU, the time-to-match measurement is estimated via a linear interpolation between the time at which the better solution is obtained and the time at which the worse solution, preceding it, is obtained.

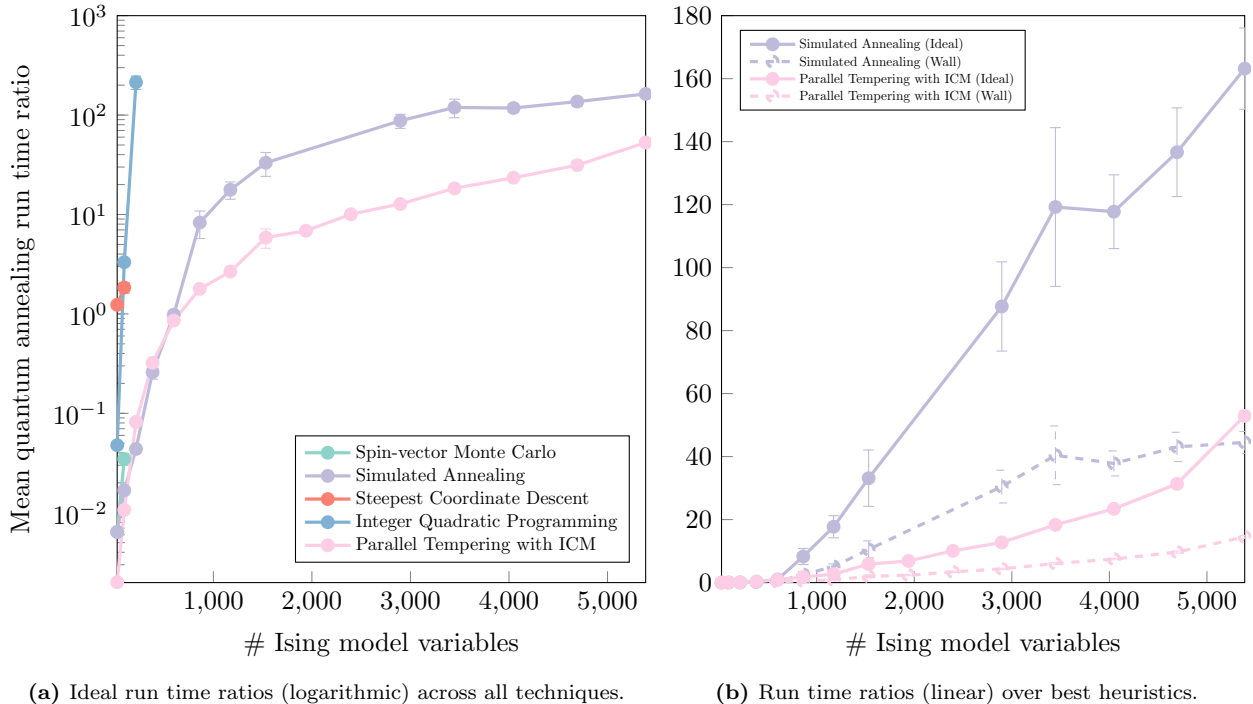


Figure 2: Estimated relative computation times (“run time ratios”) required for classical algorithms to match the solution quality of the `Advantage_system4.1` QPU as a function of problem size. Each point represents a mean computed over 50 random CBFM-P instances per problem size. Error bars correspond to standard errors of each mean run time ratio, and points are plotted only if the solver could match QA objectives for all 50 instances. The computational benefits of the QPU begin to become apparent for problems with around 1,000 decision variables, and these run time benefits increase steadily with problem size.

The results of conducting these scaling experiments and analyses are summarized in Figure 2. Figure 2a illustrates the idealized run time improvements (i.e., without including communication overheads) as a function of the number of variables in the Ising model. It is clear that the problem scale has a large impact on the usefulness of QA hardware. For small problem sizes (e.g., less than 500 variables), the QPU run time is greater than most of the classical algorithms, as indicated by a run time ratio less than 10^0 . For instances containing roughly 1,000 variables or more, the QA hardware begins to have run time performance benefits, and only the best classical heuristics, i.e., PT-ICM and SA, are capable of matching the QA hardware’s solution quality, albeit sometimes after a significant amount of time. Note that points are excluded from Figure 2a if a solver did not match the QA solution quality for all 50 instances. For example, SA matched the solution quality for only 49 of 50 instances for PEGASUS lattice sizes of 9 and 10, and hence these points are excluded from this plot.

For the two most competitive classical methods, PT-ICM and SA, Figure 2b shows that the run time benefits of the QA hardware increase steadily with problem size. This trend holds when considering both the idealized computation setting (solid lines) and the real-world setting that includes communication and scheduling overheads (dashed lines). In particular, the estimated $15\times$ run time ratio for the largest problem size is encouraging, as this suggests that the solutions identified by the QPU, even when accessed via a cloud computing service, can be obtained quickly enough to accelerate the performance of classical heuristic methods.

4 Limitations and Opportunities

Sections 3.1 and 3.2 provide evidence that there exist classes of Ising models where available QA hardware can provide run time performance improvements over classical alternatives. This is an encouraging result, but it is also important to recognize some limitations of this study and available QA hardware.

Limitations of This Study: The foremost limitation of this work is that it considers Ising models that are hardware-native. Such models provide best-case scenarios for QA hardware and, thus far, have not reflected sparsity patterns of realistic combinatorial optimization tasks. Although this work demonstrates an important *necessary* condition for having a performance benefit on practical problems, it is not a *sufficient* condition. Benchmarking real-world problems is required to show that these benefits can be also realized in that context.

We also note that most of the classical algorithms employed in this work did not effectively exploit parallelism, and all except SVMC and PT-ICM used their single-threaded variants. Parallelism of classical algorithms may reduce or eliminate the performance benefits presented in this work. Further, the benchmarks considered in this study did not evaluate other novel computing technologies or special-purpose hardware (e.g., [60, 32, 57, 37, 53]), which could provide improved performance on CBFM-P instances. Both of these avenues should be explored in future work to improve heuristic algorithms and better exploit computational resources.

Finally, we also recognize that this study does not attempt to demonstrate nor assert the much sought-after *scaling advantage* from quantum annealing [70], even for the contrived class of CBFM-P instances that are considered. This work has provided encouraging initial evidence of a class of Ising models where QA hardware can provide a practical, constant factor performance improvement over available classical algorithms.

Limitations of Current QA Hardware: The primary limitation of the QA hardware identified in this study is that it appears to approach a limit on solution quality for the largest CBFM-P instance class, i.e., around 0.20% from the best-known solution. More evidence for this behavior is provided in Appendix C. As such, this work adopted a *time-to-match* measurement of performance, which is atypical for an optimization benchmarking study. Additional research is required to develop extensions of the simple QA optimization protocols used in this work to understand if the hardware can achieve solutions that are within 0.01% of global optimality, which would make this hardware’s performance consistent with standard optimality tolerances used by commercial optimization tools. QA hardware improvements to reduce noise and integrated control errors would also serve to further close this gap.

Future Opportunities: Despite the limitations of this work and current QA hardware, our results provide encouraging evidence that QA hardware is reaching a point where existing classical optimization algorithms can be practically outperformed, especially over very short timescales. If QA hardware continues to increase in the number of qubits and hardware graph connectivity while also reducing noise properties, it is reasonable to expect that the performance gap on hardware-native problem instances will continue to increase, as suggested by the results of Section 3.2. Recently, D-Wave Systems announced their plans to develop an ADVANTAGE 2 QPU, which will support over 7,000 decision variables and a denser hardware graph [15]. If the trends observed in this work continue on this new platform, identifying even more dramatic performance gains should be possible. Acknowledging these anticipated hardware improvements, as well as the empirical findings of this study, revisiting the topic of demonstrating a QA scaling advantage (as in [19, 2]) is a natural next step to establish a stronger case for a fundamental performance benefit of the QA computing model for combinatorial optimization.

5 Conclusion

After roughly twenty years of research and development and ten years of focused commercial development, we believe quantum annealing technology has reached a level of technical maturity and performance that warrants serious consideration by the operations research community. This work has shown, for the first time,

an order-of-magnitude run time performance benefit for quantum annealing over a wide range of classical alternatives, even when accounting for the substantial overheads involved in the practical usage of commercial quantum annealing services. Nonetheless, significant open challenges remain in translating these performance results into benefits for practical optimization tasks. There may be significant unrealized opportunities to hybridize this new computing technology into existing mathematical programming algorithms and impact real-world optimization challenges. We sincerely hope that this work will inspire the operations research community to increase its consideration of the quantum annealing computing model and continue exploring how it can potentially benefit mathematical optimization algorithms and practical applications.

6 Acknowledgment

All work at Los Alamos National Laboratory was conducted under the auspices of the National Nuclear Security Administration of the U.S. Department of Energy under Contract No. 89233218CNA000001. This research used resources provided by the Los Alamos National Laboratory Institutional Computing Program and was supported by the Laboratory Directed Research and Development program under the projects 20210114ER and 20210674ECR. This material is based upon work supported by the National Science Foundation under Grant No. 2037755.

References

- [1] Scott Aaronson. Insert D-Wave post here. <https://web.archive.org/web/20220305233421/https://scottaaronson.blog/?p=3192>, 2017. Accessed: 2022-04-28.
- [2] Tameem Albash and Daniel A. Lidar. Demonstration of a scaling advantage for a quantum annealer over simulated annealing. *Phys. Rev. X*, 8:031016, Jul 2018.
- [3] Tameem Albash, Walter Vinci, Anurag Mishra, Paul A. Warburton, and Daniel A. Lidar. Consistency tests of classical and quantum models for a quantum annealer. *Phys. Rev. A*, 91:042314, Apr 2015.
- [4] Flavio Baccari, Christian Gogolin, Peter Wittek, and Antonio Ací. Verifying the output of quantum optimizers with ground-state energy lower bounds. *Physical Review Research*, 2(4), oct 2020.
- [5] John E Beasley. Heuristic algorithms for the unconstrained binary quadratic programming problem. Technical report, Management School, Imperial College, 1998.
- [6] A J Berkley, M W Johnson, P Bunyk, R Harris, J Johansson, T Lanting, E Ladizinsky, E Tolkaheva, M H S Amin, and G Rose. A scalable readout system for a superconducting adiabatic quantum optimization system. *Superconductor Science and Technology*, 23(10):105014, sep 2010.
- [7] Alain Billionnet and Sourour Elloumi. Using a mixed integer quadratic programming solver for the unconstrained quadratic 0-1 problem. *Mathematical Programming*, 109(1):55–68, January 2007.
- [8] Sergio Boixo, Troels F. Rønnow, Sergei V. Isakov, Zhihui Wang, David Wecker, Daniel A. Lidar, John M. Martinis, and Matthias Troyer. Evidence for quantum annealing with more than one hundred qubits. *Nature Physics*, 10(3):218–224, Mar 2014.
- [9] Kelly Boothby, Paul Bunyk, Jack Raymond, and Aidan Roy. Next-generation topology of D-Wave quantum processors. *arXiv e-prints*, page arXiv:2003.00133, February 2020.
- [10] M. Born and V. Fock. Beweis des adiabatensatzes. *Zeitschrift für Physik*, 51(3):165–180, 1928.
- [11] Carleton Coffrin, Harsha Nagarajan, and Russell Bent. Evaluating Ising processing units with integer programming. In Louis-Martin Rousseau and Kostas Stergiou, editors, *Integration of Constraint Programming, Artificial Intelligence, and Operations Research*, pages 163–181, Cham, 2019. Springer International Publishing.

- [12] E. J. Crosson and D. A. Lidar. Prospects for quantum enhancement with diabatic quantum annealing. *Nature Reviews Physics*, 3(7):466–489, 2021.
- [13] Philip J. D. Crowley and A. G. Green. Anisotropic Landau-Lifshitz-Gilbert models of dissipation in qubits. *Phys. Rev. A*, 94:062106, Dec 2016.
- [14] D-Wave Systems. D-Wave system documentation. <https://docs.dwavesys.com/docs/latest/>, 2020. Accessed: 2021-03-17.
- [15] D-Wave Systems. Clarity: A roadmap for the future of quantum computing. https://web.archive.org/web/20220320053047/https://www.dwavesys.com/media/xvjpraig/clarity-roadmap_digital_v2.pdf, 2021. Accessed: 2022-04-26.
- [16] D-Wave Systems. DWAVE-NEAL. <https://docs.ocean.dwavesys.com/projects/neal/en/latest/>, 2022. Accessed: 2022-03-15.
- [17] D-Wave Systems. DWAVE-TABU. <https://docs.ocean.dwavesys.com/projects/d-wave-systems-dwave-tabu/en/latest>, 2022. Accessed: 2022-05-02.
- [18] Sanjeeb Dash. A note on QUBO instances defined on Chimera graphs. 2013.
- [19] Vasil S. Denchev, Sergio Boixo, Sergei V. Isakov, Nan Ding, Ryan Babbush, Vadim Smelyanskiy, John Martinis, and Hartmut Neven. What is the computational value of finite-range tunneling? *Phys. Rev. X*, 6:031015, Aug 2016.
- [20] Deepak Dhar, Prabodh Shukla, and James P Sethna. Zero-temperature hysteresis in the random-field Ising model on a Bethe lattice. *Journal of Physics A: Mathematical and General*, 30(15):5259–5267, aug 1997.
- [21] Iain Dunning, Swati Gupta, and John Silberholz. What works best when? A systematic evaluation of heuristics for max-cut and QUBO. *INFORMS Journal on Computing*, 30(3), 2018.
- [22] Edward Farhi, Jeffrey Goldstone, and Sam Gutmann. Quantum adiabatic evolution algorithms versus simulated annealing. *arXiv e-prints*, pages quant-ph/0201031, January 2002.
- [23] Edward Farhi, Jeffrey Goldstone, Sam Gutmann, Joshua Lapan, Andrew Lundgren, and Daniel Preda. A quantum adiabatic evolution algorithm applied to random instances of an NP-complete problem. *Science*, 292(5516):472–475, 2001.
- [24] Edward Farhi, Jeffrey Goldstone, Sam Gutmann, and Michael Sipser. Quantum computation by adiabatic evolution, 2000.
- [25] Richard P. Feynman. Simulating physics with computers. *International Journal of Theoretical Physics*, 21(6):467–488, Jun 1982.
- [26] A.B. Finnila, M.A. Gomez, C. Sebenik, C. Stenson, and J.D. Doll. Quantum annealing: A new method for minimizing multidimensional functions. *Chemical Physics Letters*, 219(5):343 – 348, 1994.
- [27] M.P.C. Fossorier, M. Mihaljevic, and H. Imai. Reduced complexity iterative decoding of low-density parity check codes based on belief propagation. *IEEE Transactions on Communications*, 47(5):673–680, 1999.
- [28] Giovanni Gallavotti. *Statistical Mechanics: A Short Treatise*. Springer Science & Business Media, 2013.
- [29] Charlie J. Geyer. Parallel tempering. In E. M. Keramidas and S. M. Kaufman, editors, *Computing Science and Statistics Proceedings of the 23rd Symposium on the Interface*, page 156, New York, 1991. American Statistical Association.
- [30] Roy J. Glauber. Time-dependent statistics of the Ising model. *Journal of Mathematical Physics*, 4(2):294–307, 1963.

- [31] Fred Glover and Manuel Laguna. *Tabu Search*, pages 2093–2229. Springer US, Boston, MA, 1998.
- [32] Hayato Goto, Kosuke Tatsumura, and Alexander R. Dixon. Combinatorial optimization by simulating adiabatic bifurcations in nonlinear Hamiltonian systems. *Science Advances*, 5(4):eaav2372, 2019.
- [33] R. Harris, M. W. Johnson, T. Lanting, A. J. Berkley, J. Johansson, P. Bunyk, E. Tolkacheva, E. Ladizinsky, N. Ladizinsky, T. Oh, F. Cioata, I. Perminov, P. Spear, C. Enderud, C. Rich, S. Uchaikin, M. C. Thom, E. M. Chapple, J. Wang, B. Wilson, M. H. S. Amin, N. Dickson, K. Karimi, B. Macready, C. J. S. Truncik, and G. Rose. Experimental investigation of an eight-qubit unit cell in a superconducting optimization processor. *Phys. Rev. B*, 82:024511, Jul 2010.
- [34] W. K. Hastings. Monte Carlo sampling methods using Markov chains and their applications. *Biometrika*, 57(1):97–109, April 1970.
- [35] Philipp Hauke, Helmut G Katzgraber, Wolfgang Lechner, Hidetoshi Nishimori, and William D Oliver. Perspectives of quantum annealing: methods and implementations. *Reports on Progress in Physics*, 83(5):054401, may 2020.
- [36] Itay Hen, Joshua Job, Tameem Albash, Troels F. Rønnow, Matthias Troyer, and Daniel A. Lidar. Probing for quantum speedup in spin-glass problems with planted solutions. *Phys. Rev. A*, 92:042325, Oct 2015.
- [37] Toshimori Honjo, Tomohiro Sonobe, Kensuke Inaba, Takahiro Inagaki, Takuya Ikuta, Yasuhiro Yamada, Takushi Kazama, Koji Enbutsu, Takeshi Umeki, Ryoichi Kasahara, Ken ichi Kawarabayashi, and Hiroki Takesue. 100,000-spin coherent Ising machine. *Science Advances*, 7(40):eabh0952, 2021.
- [38] Jérôme Houdayer. A cluster Monte Carlo algorithm for 2-dimensional spin glasses. *Eur. Phys. J. B*, 22(4):479–484, 2001.
- [39] Koji Hukushima and Koji Nemoto. Exchange Monte Carlo method and application to spin glass simulations. *Journal of the Physical Society of Japan*, 65(6):1604–1608, 1996.
- [40] Sabine Jansen, Mary-Beth Ruskai, and Ruedi Seiler. Bounds for the adiabatic approximation with applications to quantum computation. *Journal of Mathematical Physics*, 48(10):102111, 2007.
- [41] Joshua Job and Daniel Lidar. Test-driving 1000 qubits. *Quantum Science and Technology*, 3(3):030501, jun 2018.
- [42] M. W. Johnson, M. H. S. Amin, S. Gildert, T. Lanting, F. Hamze, N. Dickson, R. Harris, A. J. Berkley, J. Johansson, P. Bunyk, E. M. Chapple, C. Enderud, J. P. Hilton, K. Karimi, E. Ladizinsky, N. Ladizinsky, T. Oh, I. Perminov, C. Rich, M. C. Thom, E. Tolkacheva, C. J. S. Truncik, S. Uchaikin, J. Wang, B. Wilson, and G. Rose. Quantum annealing with manufactured spins. *Nature*, 473(7346):194–198, 2011.
- [43] M W Johnson, P Bunyk, F Maibaum, E Tolkacheva, A J Berkley, E M Chapple, R Harris, J Johansson, T Lanting, I Perminov, E Ladizinsky, T Oh, and G Rose. A scalable control system for a superconducting adiabatic quantum optimization processor. *Superconductor Science and Technology*, 23(6):065004, apr 2010.
- [44] Tadashi Kadowaki and Hidetoshi Nishimori. Quantum annealing in the transverse Ising model. *Phys. Rev. E*, 58:5355–5363, Nov 1998.
- [45] Tosio Kato. On the adiabatic theorem of quantum mechanics. *Journal of the Physical Society of Japan*, 5(6):435–439, 1950.
- [46] Helmut G Katzgraber, Simon Trebst, David A Huse, and Matthias Troyer. Feedback-optimized parallel tempering Monte Carlo. *Journal of Statistical Mechanics: Theory and Experiment*, 2006(03):P03018–P03018, mar 2006.

- [47] Andrew D. King, Sei Suzuki, Jack Raymond, Alex Zucca, Trevor Lanting, Fabio Altomare, Andrew J. Berkley, Sara Ejtemaee, Emile Hoskinson, Shuiyuan Huang, Eric Ladizinsky, Allison MacDonald, Gaelen Marsden, Travis Oh, Gabriel Poulin-Lamarre, Mauricio Reis, Chris Rich, Yuki Sato, Jed D. Whittaker, Jason Yao, Richard Harris, Daniel A. Lidar, Hidetoshi Nishimori, and Mohammad H. Amin. Coherent quantum annealing in a programmable 2000-qubit Ising chain, 2022.
- [48] James King, Sheir Yarkoni, Mayssam M Nevisi, Jeremy P Hilton, and Catherine C McGeoch. Benchmarking a quantum annealing processor with the time-to-target metric. *arXiv preprint arXiv:1508.05087*, 2015.
- [49] James King, Sheir Yarkoni, Jack Raymond, Isil Ozfidan, Andrew D. King, Mayssam Mohammadi Nevisi, Jeremy P. Hilton, and Catherine C. McGeoch. Quantum annealing amid local ruggedness and global frustration, 2017.
- [50] John R. Klauder. Path integrals and stationary-phase approximations. *Phys. Rev. D*, 19:2349–2356, Apr 1979.
- [51] Gary Kochenberger, Jin-Kao Hao, Fred Glover, Mark Lewis, Zhipeng Lü, Haibo Wang, and Yang Wang. The unconstrained binary quadratic programming problem: a survey. *Journal of Combinatorial Optimization*, 28(1):58–81, Jul 2014.
- [52] Aminata Kone and David A. Kofke. Selection of temperature intervals for parallel-tempering simulations. *The Journal of Chemical Physics*, 122(20):206101, 2005.
- [53] Matthew Kowalsky, Tameem Albash, Itay Hen, and Daniel A Lidar. 3-regular three-XORSAT planted solutions benchmark of classical and quantum heuristic optimizers. *Quantum Science and Technology*, 7(2):025008, feb 2022.
- [54] Andrew Lucas. Ising formulations of many NP problems. *Frontiers in Physics*, 2, 2014.
- [55] Salvatore Mandrà and Helmut G Katzgraber. A deceptive step towards quantum speedup detection. *Quantum Science and Technology*, 3(4):04LT01, jul 2018.
- [56] Salvatore Mandrà, Zheng Zhu, Wenlong Wang, Alejandro Perdomo-Ortiz, and Helmut G. Katzgraber. Strengths and weaknesses of weak-strong cluster problems: A detailed overview of state-of-the-art classical heuristics versus quantum approaches. *Phys. Rev. A*, 94:022337, Aug 2016.
- [57] Satoshi Matsubara, Motomu Takatsu, Toshiyuki Miyazawa, Takayuki Shibasaki, Yasuhiro Watanabe, Kazuya Takemoto, and Hiroataka Tamura. Digital annealer for high-speed solving of combinatorial optimization problems and its applications. In *2020 25th Asia and South Pacific Design Automation Conference (ASP-DAC)*, pages 667–672, 2020.
- [58] Catherine McGeoch and Pau Farre. The D-Wave Advantage system: An overview. *Technical Report*, 2020.
- [59] Catherine C. McGeoch and Cong Wang. Experimental evaluation of an adiabatic quantum system for combinatorial optimization. In *Proceedings of the ACM International Conference on Computing Frontiers*, CF '13, pages 23:1–23:11, New York, NY, USA, 2013. ACM.
- [60] Peter L. McMahon, Alireza Marandi, Yoshitaka Haribara, Ryan Hamerly, Carsten Langrock, Shuhei Tamate, Takahiro Inagaki, Hiroki Takesue, Shoko Utsunomiya, Kazuyuki Aihara, Robert L. Byer, M. M. Fejer, Hideo Mabuchi, and Yoshihisa Yamamoto. A fully programmable 100-spin coherent Ising machine with all-to-all connections. *Science*, 354(6312):614–617, 2016.
- [61] Nicholas Metropolis, Arianna W. Rosenbluth, Marshall N. Rosenbluth, Augusta H. Teller, and Edward Teller. Equation of state calculations by fast computing machines. *The Journal of Chemical Physics*, 21(6):1087–1092, 1953.
- [62] Marc Mezard and Andrea Montanari. *Information, Physics, and Computation*. Oxford University Press, 2009.

- [63] Masoud Mohseni, Daniel Eppens, Johan Strumpfer, Raffaele Marino, Vasil Denchev, Alan K. Ho, Sergei V. Isakov, Sergio Boixo, Federico Ricci-Tersenghi, and Hartmut Neven. Nonequilibrium Monte Carlo for unfreezing variables in hard combinatorial optimization. *arXiv e-prints*, page arXiv:2111.13628, November 2021.
- [64] Jon Nelson, Marc Vuffray, Andrey Y. Lokhov, and Carleton Coffrin. Single-qubit fidelity assessment of quantum annealing hardware. *IEEE Transactions on Quantum Engineering*, 2:1–10, 2021.
- [65] Gintaras Palubeckis. Multistart Tabu search strategies for the unconstrained binary quadratic optimization problem. *Annals of Operations Research*, 131(1):259–282, October 2004.
- [66] Yuchen Pang, Carleton Coffrin, Andrey Y Lokhov, and Marc Vuffray. The potential of quantum annealing for rapid solution structure identification. *Constraints*, 26(1):1–25, 2021.
- [67] Jean Francois Puget. D-Wave vs CPLEX comparison. Part 2: QUBO. https://web.archive.org/web/20170702140136/https://www.ibm.com/developerworks/community/blogs/jfp/entry/d_wave_vs_cplex_comparison_part_2_qubo?lang=en, 2013. Accessed: 2022-04-27.
- [68] P. Ray, B. K. Chakrabarti, and Arunava Chakrabarti. Sherrington-Kirkpatrick model in a transverse field: Absence of replica symmetry breaking due to quantum fluctuations. *Phys. Rev. B*, 39:11828–11832, June 1989.
- [69] Ignacio Rozada, Maliheh Aramon, Jonathan Machta, and Helmut G. Katzgraber. Effects of setting temperatures in the parallel tempering Monte Carlo algorithm. *Phys. Rev. E*, 100:043311, Oct 2019.
- [70] Troels F. Rønnow, Zhihui Wang, Joshua Job, Sergio Boixo, Sergei V. Isakov, David Wecker, John M. Martinis, Daniel A. Lidar, and Matthias Troyer. Defining and detecting quantum speedup. *Science*, 345(6195):420–424, 2014.
- [71] Giuseppe E. Santoro, Roman Martoňák, Erio Tosatti, and Roberto Car. Theory of quantum annealing of an Ising spin glass. *Science*, 295(5564):2427–2430, 2002.
- [72] Alex Selby. QUBO-CHIMERA. <https://github.com/alex1770/QUBO-Chimera>, 2013.
- [73] Alex Selby. Efficient subgraph-based sampling of ising-type models with frustration, 2014.
- [74] Seung Woo Shin, Graeme Smith, John A Smolin, and Umesh Vazirani. How “quantum” is the D-Wave machine? *arXiv preprint arXiv:1401.7087*, 2014.
- [75] Robert H. Swendsen and Jian-Sheng Wang. Replica Monte Carlo simulation of spin-glasses. *Phys. Rev. Lett.*, 57:2607–2609, November 1986.
- [76] Peter J. M. van Laarhoven and Emile H. L. Aarts. *Simulated annealing*, pages 7–15. Springer Netherlands, Dordrecht, 1987.
- [77] Marc Vuffray. The cavity method in coding theory. Technical report, EPFL, 2014.
- [78] Marc Vuffray, Carleton Coffrin, Yaroslav A. Kharkov, and Andrey Y. Lokhov. Programmable quantum annealers as noisy Gibbs samplers. *PRX Quantum*, 3:020317, Apr 2022.
- [79] Tristan Zaborniak and Rogério de Sousa. Benchmarking Hamiltonian noise in the D-Wave quantum annealer. *IEEE Transactions on Quantum Engineering*, 2:1–6, 2021.
- [80] Zheng Zhu, Andrew J. Ochoa, and Helmut G. Katzgraber. Efficient cluster algorithm for spin glasses in any space dimension. *Phys. Rev. Lett.*, 115:077201, August 2015.

LA-UR-22-29705

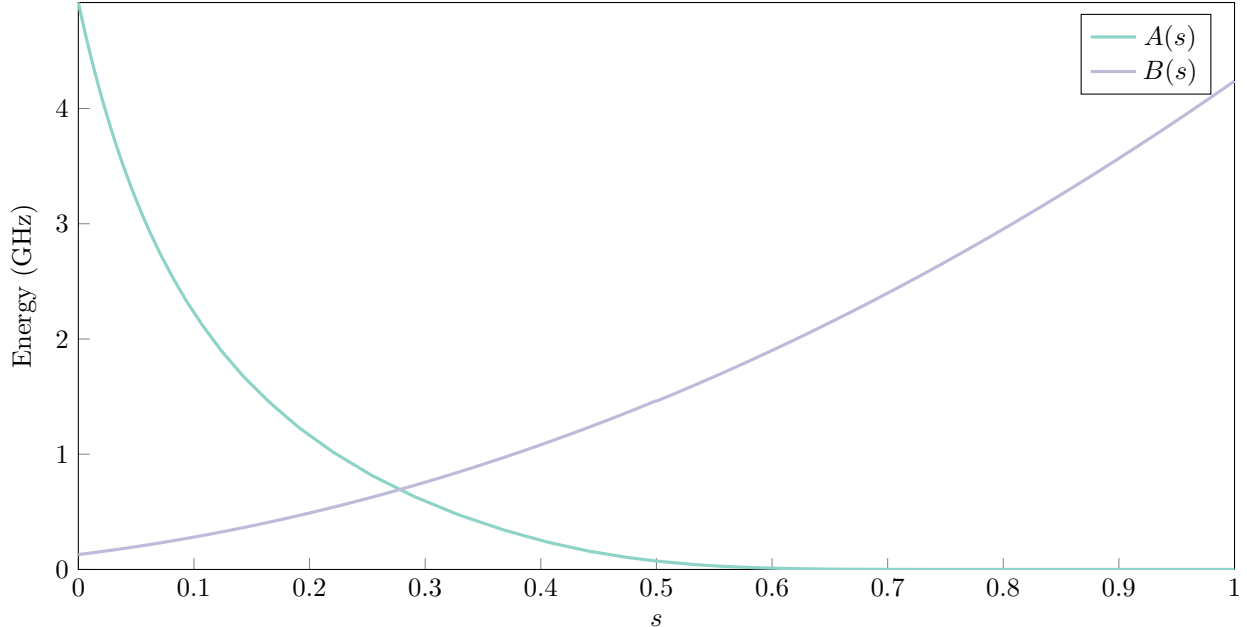


Figure 3: Annealing schedule used by D-Wave Systems’ `Advantage_system4.1` QPU used throughout this study, in units where the Planck constant set to one.

A D-Wave Advantage System Details

In an ideal setting, a QA hardware device would provide the user control over the Ising models and annealing schedules that are executed. However, available QA hardware impose restrictions on the classes of Ising models and annealing schedules that can be considered per the hardware’s architecture. In this paper, we used the `Advantage_system4.1` QPU, which is based on the `ADVANTAGE` architecture [9]. This system implements the transverse-field Ising model,

$$E(s) = -A(s) \sum_{i \in \mathcal{N}} \hat{\sigma}_i^x + B(s) \left(\sum_{(i,j) \in \mathcal{E}^H} J_{ij} \hat{\sigma}_i^z \hat{\sigma}_j^z - \sum_{i \in \mathcal{N}} h_i \hat{\sigma}_i^z \right), \quad (6)$$

where $\hat{\sigma}^x$ and $\hat{\sigma}^z$ are the Pauli operators for the x and z bases, respectively, and the Ising model of interest is encoded in the z basis. The hardware has a fixed global annealing schedule shown in Figure 3 and a qubit connectivity graph known as `PEGASUS`, containing a total of 5,387 qubits. Figure 4 illustrates a `PEGASUS` graph topology with a lattice “size parameter” of two. A `PEGASUS unit cell` contains twenty-four qubits (here, the three diagonal clusters of eight), with each qubit coupled to one similarly aligned qubit *within* the cell and two similarly aligned qubits *in adjacent cells*. An `ADVANTAGE` QPU is a lattice of 16×16 such unit cells. This example illustrates that the use of QA is limited to Ising models that are *topologically consistent* with the QPU used and *size-restricted* by its number of qubits. In this work, we only consider Ising models that are subsets of this hardware graph, i.e., hardware-native Ising models. This allows us to avoid effects caused by the *embedding* problem, which is defined as mapping a desired problem structure onto this hardware graph.

Even if the Ising model is topologically consistent, achieving a globally optimal solution to Problem (2) using QA is often difficult at large scales. As explained in Section 2, QA has been theoretically shown to minimize the energy of specific target Ising models. Experimentally, however, this is not always the case. One reason is the unavoidable corruption of the quantum system from its external environment. For example, as previously stated in Section 2, QPUs are known to suffer from a wide range of *integrated control errors*, including susceptibility to background noise, flux noise, digital-to-analog conversion, and variable scales and coefficient biases across qubits [64].

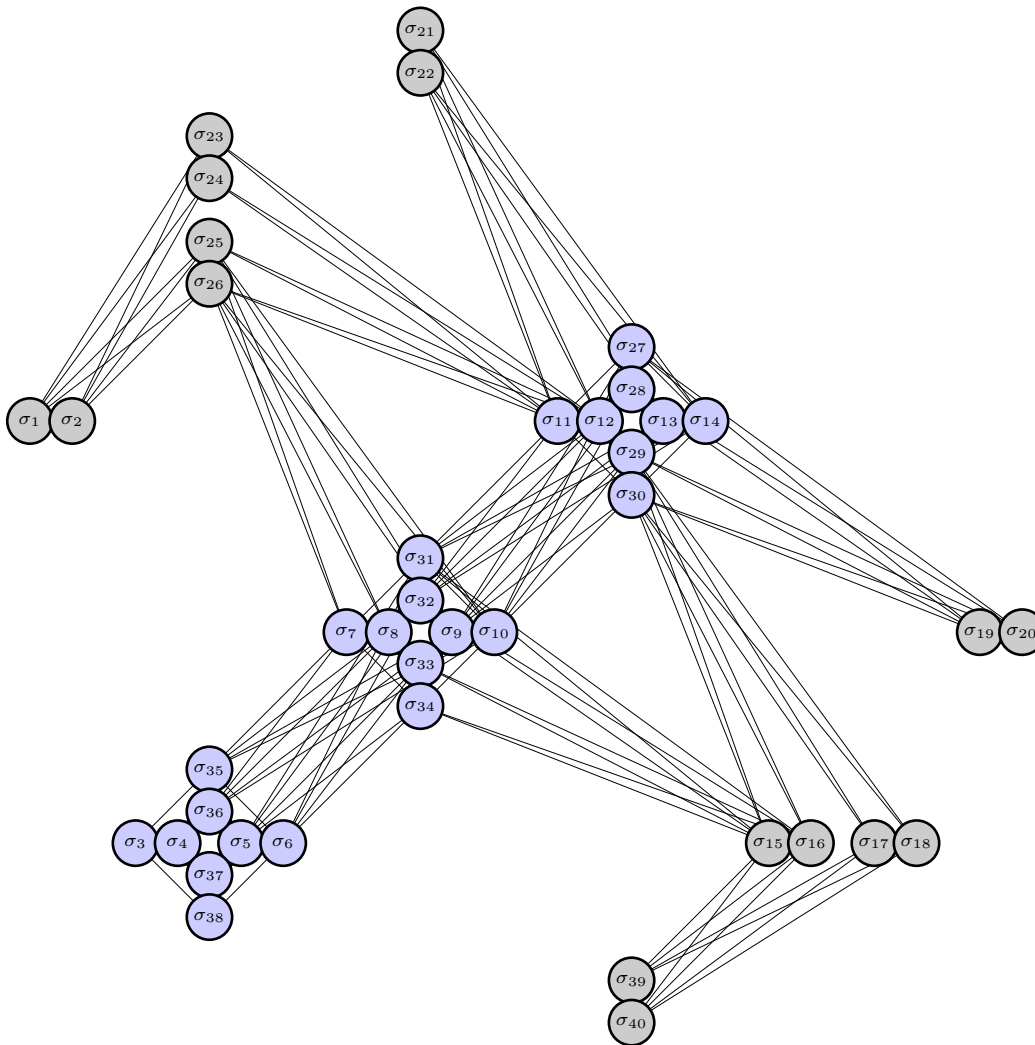


Figure 4: Topology of a PEGASUS graph with a size parameter of two, where blue nodes comprise a unit cell.

It is also important to note that QPUs, such as the ADVANTAGE, often distinguish between the tasks of *optimization* and *sampling*. The former aims at determining a solution to Problem (2), while the latter aims at characterizing the *energy landscape* of an Ising model. In practice, since quantum annealing does not experimentally guarantee convergence to a global optimum, optimization is performed by conducting multiple *anneal-read cycles* (or “reads”) for the target Ising model. Each read provides an assignment of the decision variables, which may or may not be the true global optimum of Problem (2) but which tends to be high-quality (e.g., within one percent of optimality). The best encountered solution is then extracted by computing the minimum of these multiple reads.

In this paper, we consider only two key parameters for the configuration of a QPU, and we ignore any environmental factors that are beyond our control. The first parameter is the number of anneal-read cycles performed to obtain a solution to Problem (2). Here, a larger number generally corresponds to a higher likelihood of sampling the true ground state, i.e., as the number of reads increases, solution quality also tends to increase. The second parameter is the *annealing time* that defines *each* anneal-read cycle, which is on the order of microseconds. Here, longer anneal times typically encourage convergence of the QPU to higher-quality solutions, as would be expected from quantum annealing theory. Empirical evidence of this

tendency is provided in Appendix C.

B Optimization Methods

In the interest of clarity, Section 3 briefly introduced five established and distinct solution approaches for solving the proposed CBFM-P problem instances. However, in the development of this work, we considered ten different solution approaches. In this section, we discuss all ten methods that were considered and provide additional details regarding how each was configured. The algorithms are divided into two broad categories: *complete search methods*, which, given sufficient time, provide proofs of global optimality, and *local search methods*, which are heuristics with no guarantees nor bounds on solution quality. Unless noted otherwise, each of these solvers was implemented in C/C++.

B.1 Complete Search Methods

In all of the complete search methods that are considered, we leverage the bijection of Ising models and QUBO models to convert a given Ising model of interest to its equivalent QUBO form prior to its solution [11]. Preliminary experiments indicated that the QUBO formulation is advantageous for commercial mathematical programming tools, which include specialized techniques for solving problems with discrete $\{0, 1\}$ decision variables. In this work, we considered both GUROBI, version 9.1, and CPLEX, version 22.1, for solving these mathematical programming models. Both solvers were parameterized to use only one thread during solution. Solver execution time limits were varied from one to 8,192 seconds in multiples of two for each instance. All other solver parameters assumed their default values. As discussed by [67], we acknowledge that better performance may be attained with a larger number of threads and adjusting the solvers' other parameter settings.

Mathematical programming solution approaches were considered by some of the earliest QA benchmarking studies [59] and are widely recognized as an unfair point of comparison, as specialized heuristics can be much faster than these general purpose solvers [67]. However, it was shown by [11] and [66] that these solvers provide an important point of reference for ruling out easy optimization tasks, as is similarly done in this study.

B.1.1 Integer quadratic programming

The integer quadratic programming (IQP) method considered in this study consists of using black-box commercial mathematical programming software (in this case, GUROBI and CPLEX) to pose and solve the following QUBO Ising model translation:

$$\begin{aligned} \text{minimize} \quad & \sum_{(i,j) \in \mathcal{E}} c_{ij} x_i x_j + \sum_{i \in \mathcal{N}} c_i x_i + c \\ & x_i \in \{0, 1\}, \forall i \in \mathcal{N}, \end{aligned} \tag{7}$$

where c_{ij} , c_i , and c are QUBO parameters derived from the Ising model parameters of Equation (1).

B.1.2 Integer linear programming

The integer linear programming (ILP) model is an equivalent reformulation of the IQP model, where each variable product, $x_i x_j$, is lifted into a new variable space, x_{ij} . For each new variable, constraints are used to model each conjunctive relationship, i.e., $x_{ij} = x_i \wedge x_j$. Notably, this new problem contains no quadratic terms in the objective, and all constraints are affine. The ILP reformulation of the IQP formulation discussed

in Section B.1.1 is

$$\begin{aligned}
& \text{minimize} && \sum_{(i,j) \in \mathcal{E}} c_{ij} x_{ij} + \sum_{i \in \mathcal{N}} c_i x_i + c \\
& \text{subject to} && x_i + x_j - 1 \leq x_{ij}, \forall (i, j) \in \mathcal{E} \\
& && x_{ij} \leq x_i, \forall (i, j) \in \mathcal{E} \\
& && x_{ij} \leq x_j, \forall (i, j) \in \mathcal{E} \\
& && x_i \in \{0, 1\}, \forall i \in \mathcal{N} \\
& && x_{ij} \in \{0, 1\}, \forall (i, j) \in \mathcal{E}.
\end{aligned} \tag{8}$$

This model was also evaluated in some of the earliest QA and QUBO benchmarking studies [67, 18, 7], which suggested that it is a very effective formulation for solving Ising models with sparse graphs (e.g., D-Wave’s previous CHIMERA topology). Like [66], our results indicate that IQP solvers have improved significantly over the past decade and consistently outperform ILP methods for solving QUBO problems on large problem instances. We remark that, in this study, only GUROBI (i.e., not CPLEX) was considered when solving ILP reformulations. Substantial performance differences were not anticipated when solving with CPLEX.

B.2 Local Search Methods

Although global optimization methods (e.g., IQP and ILP) are useful for measuring the quality of solutions produced by QA hardware [7, 11, 4], it is broadly accepted that local search algorithms are the most appropriate points of computational comparison for QA methods [1]. Given that an enumeration of all local search methods would be an incredibly large and impractical undertaking, this work focuses on a set of the most common or readily available approaches: greedy search via steepest coordinate descent, tabu search, messaging passing, Markov chain Monte Carlo, simulated annealing, spin-vector Monte Carlo, and parallel tempering with isoenergetic cluster moves. Next, each method is briefly described.

B.2.1 Steepest coordinate descent

The simplest heuristic algorithm considered in this work is a steepest coordinate descent, or greedy, approach that was implemented in Julia. This algorithm assigns variable values one-by-one, always taking an assignment that most decreases the objective. Specifically, the approach begins with unassigned values, i.e., $\sigma_i = 0$, for all $i \in \mathcal{N}$, then repeatedly applies the following assignment logic until all variables have been assigned a value of -1 or 1 :

$$i, v = \arg \min \{E(\sigma_1, \dots, \sigma_{i-1}, v, \sigma_{i+1}, \dots, \sigma_N) : i \in \mathcal{N}, v \in \{-1, 1\}\} \tag{9a}$$

$$\sigma_i = v \tag{9b}$$

In each application of the above rule, ties in the arg min are broken at random, giving rise to potentially stochastic outcomes. Once all variables have been assigned their values via this rule, the algorithm is repeated until a run time limit has been reached, and only the best discovered solution is returned. This approach is fast and effective on Ising models with minimal amounts of frustration. In our work, the wall-clock time limit of the steepest coordinate descent algorithm was varied from one to 8,192 seconds in multiples of two for each problem instance to understand solution improvement.

B.2.2 Tabu search

Tabu search is a metaheuristic commonly used for solving combinatorial optimization problems [31]. Like other local methods, tabu search considers a “move” operator that, for a given solution, generates a number of other possible solutions (i.e., the solution’s “neighborhood”). The “best” solution from this neighborhood is then selected, and the process repeats. To prevent cycling, a list of “tabu moves” is employed, which prohibits moves that would lead to revisiting a previously-encountered solution. This list is updated as the algorithm progresses, i.e., new moves are added to the list, and moves with a large “tabu tenure” are discarded. Tabu moves are, however, sometimes allowed if they lead to an improved solution [5].

In this study, we used an open-source implementation of the MST2 multistart tabu search algorithm of [65], provided by [17], which is specialized for solving QUBOs. For brevity, we forgo details of this algorithm.

However, in our work, for each problem instance, the number of “reads,” `num_reads`, was varied between one and 2,048 in multiples of two, and the total run time per “read,” `timeout`, was limited to a fixed value of one second. For the largest instances studied, the most time-intensive parameterizations resulted in execution times of nearly one hour.

B.2.3 Message passing

The message-based min-sum (MS) algorithm is an adaptation of the belief propagation algorithm for solving minimization problems over networks [27, 62]. A key property of the MS algorithm is its ability to identify global minima of cost functions over networks with tree-like structures, i.e., if no cycles are formed by the interactions in \mathcal{E} . In the more general case, MS is a heuristic minimization method [62]. Nonetheless, it remains a popular heuristic technique, favored in communication systems for its low computational cost and performance on tree-like networks [77].

For the model we consider, i.e., Problem (2), the MS messages, $\epsilon_{i \rightarrow j}$, are computed iteratively along *directed* edges, $i \rightarrow j$ and $j \rightarrow i$, for each $(i, j) \in \mathcal{E}$ according to the min-sum equations

$$\text{SSL}(x, y) = \min(x, y) - \min(-x, y) - x \quad (10a)$$

$$\epsilon_{i \rightarrow j}^{t+1} = \text{SSL} \left(2J_{ij}, 2h_i + \sum_{k \in \mathcal{E}(i) \setminus j} \epsilon_{k \rightarrow j}^t \right). \quad (10b)$$

Here, $\mathcal{E}(i) \setminus j$ denotes the neighbors of i without j , and SSL denotes the symmetric saturating linear (SSL) transfer function. Once a fixed point of Equation (10b) is obtained or a prescribed termination criterion is achieved (e.g., a time limit), the MS algorithm outputs the configuration

$$\bar{\sigma}_i = -\text{sign} \left(2h_i + \sum_{k \in \mathcal{E}(i)} \epsilon_{k \rightarrow j} \right). \quad (11)$$

If the argument of sign is zero, a value of 1 or -1 is assigned randomly with equal probability.

This algorithm is implemented in the Python programming language. In our work, the wall-clock time limit of the algorithm was varied from one to 8,192 seconds in multiples of two for each instance.

B.2.4 Markov chain Monte Carlo

Markov chain Monte Carlo (MCMC) algorithms are a class of methods to generate samples from complex probability distributions. A natural MCMC method for solving Ising models is given by Glauber dynamics (GD), where the value of each variable is updated according to its conditional probability distribution. Glauber dynamics is often used as a method for producing samples from Ising models at *finite temperatures* [30]. This work considers the so-called *zero temperature* GD algorithm, which is the optimization variant of the GD sampling method. This method is also used in physics as a simple model for describing avalanche phenomena in magnetic materials [20]. From an optimization perspective, the approach is similar to the single-variable greedy local search algorithm previously described in Appendix B.2.1.

A step t of the GD algorithm comprises selecting each spin variable, for $i \in \mathcal{N}$, in a random order and comparing the objective of the current configuration, $\bar{\sigma}^t$, to a configuration where $\bar{\sigma}_i^t$ is flipped in sign. If the objective value is smaller in the flipped configuration, i.e., $E(\bar{\sigma}^t) > E(\bar{\sigma}_1^t, \dots, -\bar{\sigma}_i^t, \dots, \bar{\sigma}_N^t)$, then the flipped configuration is selected as the new configuration, i.e., $\bar{\sigma}^{t+1} = (\bar{\sigma}_1^t, \dots, -\bar{\sigma}_i^t, \dots, \bar{\sigma}_N^t)$. If, after visiting all of the variables, no single-variable flip can improve the current assignment, then the configuration is identified as a local minimum. The algorithm is then restarted with a new, randomly generated initial configuration. This process is repeated until a run time limit is reached.

This algorithm is implemented in the Python programming language. In our work, the wall-clock time limit of the algorithm was varied from one to 8,192 seconds in multiples of two for each instance.

B.2.5 Simulated annealing

Simulated annealing is an algorithm inspired by the process of annealing materials to produce improved structural properties, applied to the computational task of solving a combinatorial optimization problem. In

condensed matter physics, *annealing* is a physical process by which the temperature of a solid immersed in a *heat bath* is first increased, and particles of the solid randomly rearrange themselves into a liquid phase. The temperature of the heat bath is then slowly decreased, and, in an ideal case, all particles rearrange themselves to a corresponding solid lattice structure [76]. Analogously, in simulated annealing, solutions are probabilistically perturbed according to a “temperature” schedule until reaching some minimum.

The algorithm originated with [61], who proposed a Monte Carlo method for simulating the evolution of a solid to thermal equilibrium at a fixed temperature, T . Specifically, given the current state of the system, $\bar{\sigma}$, a small perturbation is selected. If the difference in energy, ΔE , between the current and perturbed states is negative, the process is continued with the new state. Otherwise, the *probability of acceptance* of the new state is $\exp\left(-\frac{\Delta E}{k_B T}\right)$, called the Metropolis criterion, where k_B is the Boltzmann constant. Simulated annealing can thus be thought of as a *sequence of Metropolis algorithms*, where the temperature is gradually decreased until reaching some termination criterion (e.g., a predefined temperature value) [76].

In this work, we employ the DWAVE-NEAL Python package, which provides an implementation of simulated annealing for general Ising model graphs. In each execution of the algorithm, the number of anneal-read cycles was set to one hundred, and the number of simulated annealing “sweeps,” or random perturbations per discrete temperature value, varied between one and 262,144 in multiples of two. All other parameters assumed their default values. For the largest Ising models considered in this study (i.e., a PEGASUS graph with a size parameter of sixteen), the longest wall-clock execution times when employing the most time-intensive parameterization were a little over an hour.

B.2.6 Spin-vector Monte Carlo

Spin-vector Monte Carlo [74] is a classical emulator of a noisy quantum annealer, where the system of qubits, i.e., \mathcal{N} , is replaced by a system of two-dimensional rotors. The system’s energy is given by

$$E(\theta, s) = -A(s) \sum_{i \in \mathcal{N}} \sin \theta_i + B(s) \left(\sum_{i \in \mathcal{N}} h_i \cos \theta_i + \sum_{(i,j) \in \mathcal{E}} J_{ij} \cos \theta_i \cos \theta_j \right), \quad (12)$$

where $s \in [0, 1]$ is the dimensionless annealing parameter; the functions $A(s)$ and $B(s)$ are taken to match those of the quantum annealer, illustrated in Figure 3; and $\{\theta_i \in [0, \pi)\}$ are the orientations of the rotors. In principle, the rotors can point along any orientation in $[0, 2\pi)$, but with this energy function, the energy is minimized by an orientation in $[0, \pi)$, which allows us to restrict each θ_i to this range of angles. Using this energy, the rotors’ orientations are updated using a fixed-temperature Metropolis-Hastings criterion. This description can be physically motivated as a description of superconducting flux qubits in the strong system-bath interaction limit [13] when using the spin-coherent path integral formalism [50, 3].

The SVMC algorithm proceeds as follows. The rotors are initialized to point along $\theta_i = \pi/2$, corresponding to the uniform superposition state. The anneal is discretized in steps of Δs such that $s_k = k\Delta s$, and at every value of s_k , a certain number of sweeps of rotor updates are performed. A sweep corresponds to attempting one Metropolis-Hastings update for each rotor. The update goes as follows. For a rotor with orientation θ_i , we randomly choose a new orientation θ'_i , and we calculate the change in energy, ΔE , associated with this new orientation and accept the update according to the Metropolis-Hastings probability [61, 34],

$$p = \min(1, \exp(-\beta(E(\theta', s) - E(\theta, s))))), \quad (13)$$

where $\beta = 3.9983 \text{ GHz}^{-1}$ is the fixed inverse temperature of the simulation, corresponding to a physical temperature of 12 mK in units where the Planck constant set to one. At the end of the anneal, the rotors are projected to Ising spins, and we can measure their energy according to Equation (1). If $\cos \theta_i > 0$, we assign a spin value of $\sigma_i = 1$, and if $\cos \theta_i < 0$, we assign a spin value of $\sigma_i = -1$. If $\cos \theta_i$ is zero, a value of 1 or -1 is assigned randomly with equal probability.

For each problem instance, we executed eight independent SVMC simulations in parallel on eight cores, reporting the lowest energy found by the eight independent runs. For each independent SVMC run in the parallel set, the number of sweeps used by the algorithm was varied from 1,000 to 8,192,000 in multiples of two. For the largest Ising models considered in this study, the longest wall-clock execution times when employing the most time-intensive parameterization were a little over an hour.

B.2.7 Parallel tempering with isoenergetic cluster moves

Parallel tempering (PT) [75, 29, 39] is a method that uses multiple Markov chain Monte Carlo simulations to improve the equilibration dynamics. Each simulation, known as a “replica,” has a unique inverse temperature, β , and its spin configuration is evolved using single-spin Monte Carlo updates. That is, a spin with value σ_i is flipped to $\sigma'_i = -\sigma_i$, and the update is accepted according to the Metropolis-Hastings probability [61, 34],

$$p = \min(1, \exp(-\beta(E(\sigma') - E(\sigma)))) . \quad (14)$$

After each replica performs a fixed number of sweeps, where a sweep corresponds to performing a single Monte Carlo update on all the spins, a parallel tempering update is performed. In a parallel tempering update, the spin configurations (or equivalently the temperatures) of two replicas are swapped according to the Metropolis-Hastings probability ([61, 34]),

$$p = \min(1, \exp((\beta_r - \beta_{r'})(E(\sigma_r) - E(\sigma_{r'})))) , \quad (15)$$

where β_r and $E(\sigma_r)$ denote the inverse temperature and energy of the spin configuration of replica r , respectively. This choice preserves detailed balance.

The isoenergetic cluster move (ICM) [80] is based on the cluster update by Houdayer [38]. Two independent parallel tempering simulations are performed. After a fixed number of Monte Carlo sweeps and the replica swaps are performed, we perform the ICM update. This move is performed on replicas with a temperature less than one. For equal temperature replicas r and r' from each PT simulation, we calculate the site overlap,

$$q_i = \sigma_i^{(r)} \sigma_i^{(r')} , \quad i \in \mathcal{N} , \quad (16)$$

where $\sigma_i^{(r)}$ is the spin configuration of the i -th site in the r -th replica. We randomly pick a spin i with $q_i = -1$, and starting from this spin, we build the largest connected (according to \mathcal{E}) cluster of spins with $q_i = -1$. All spins in this cluster are then flipped in both replicas, r and r' . According to [80], the ICM move need not be performed on all replicas, and we only implement it on replicas with an inverse temperature greater than one.

Therefore, the complete parallel tempering with isoenergetic cluster moves (PT-ICM) algorithm proceeds as follows. All the replicas of the two independent PT simulations are initialized with random spin configurations. Each replica is evolved independently, with two Monte Carlo sweeps. This is followed by a parallel tempering update for all pairs of neighboring temperatures, where the order of the parallel tempering pairs is chosen randomly. Finally, an ICM update is performed.

In our simulations, we have chosen to use 64 replicas, and we considered two inverse temperature distributions. The first is a typical geometrical distribution, untuned with respect to the instances considered throughout this work. The PT-ICM algorithm using this “default” inverse temperature distribution is represented in Figures 1 and 2, and it represents an untuned variant of the algorithm, similar to the other methods that we compare. The second “non-default” distribution considers values ranging between [0.1, 8] to achieve a swap probability of approximately 0.23 [52] between most neighboring temperature replicas at the largest system size we study, using the scheme of [69]. We illustrate this distribution in Figure 5. Further, PT-ICM results when using this distribution are postfixed with (Opt.) in subsequent figures of this appendix. We remark, however, that this choice of temperatures is not necessarily optimal [46], but it is generally considered a reasonable choice. In principle, at the smaller system sizes, we require fewer replicas to achieve the same swap probability, but we do not perform this optimization, here.

In our reported results, for each problem instance, we executed eight independent PT-ICM simulations in parallel on eight cores, and we reported the lowest energy found by the eight independent runs. For each independent PT-ICM run in the parallel set, the number of parallel tempering updates used by the algorithm, prior to termination, was varied from two to 16,384 in multiples of two. For the largest Ising models considered in this study, the longest wall-clock execution times when employing the most time-intensive parameterization were typically less than thirty minutes.

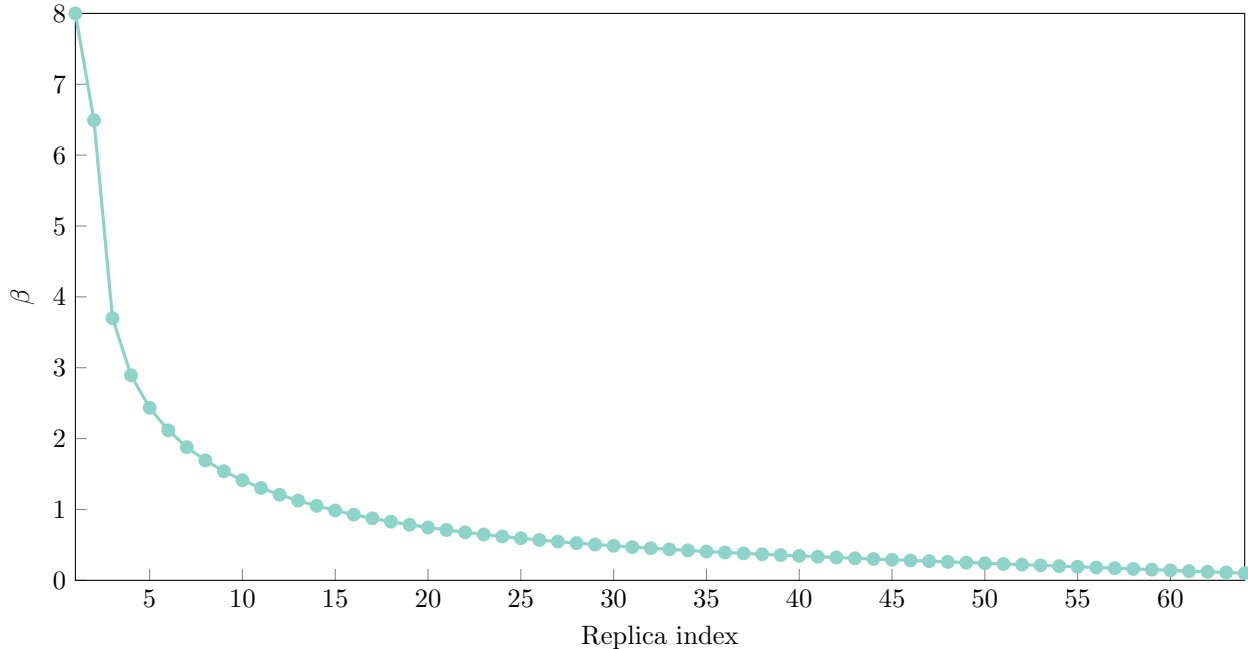


Figure 5: Inverse temperature distribution over the 64 PT-ICM replicates considered in the “tuned” variant.

C Annealing Time Sensitivity

In the quantum annealing solution approach, the annealing time, τ (μs), of the algorithm plays a critical role in solution quality [70, 2], since it is generally the case that increasing the annealing time will increase quality until a globally optimal solution is achieved. Consequently, in this work, we considered different annealing times to understand their impacts on the quality of CBFM-P solutions. This also allowed us to select a suitable value of τ .

Figure 6 shows the mean relative performance of the QA hardware over a set of 50 instances with 5,387 decision variables (PEGASUS lattice size sixteen). Here, the number of anneal-read cycles was varied between ten and 5,120 in multiples of two, resulting in a variety of idealized and wall-clock QPU execution times, displayed on the horizontal axis. The annealing time, τ , used in each solution process was also varied from 0.5 to 312.5 μs in multiples of five. The solution qualities and execution times resulting from these annealing time parameterizations are depicted by the five grayscale curves.

It is first apparent that, for a fixed number of anneal-read cycles, as the annealing time is increased, the solution quality also increases. This is encouraging, as it indicates that the QA hardware is behaving similarly to what the theory of QA predicts. However, for each increase in annealing time, there are consistent diminishing returns in terms of solution quality. In particular, between $\tau = 62.5 \mu\text{s}$ and $\tau = 312.5 \mu\text{s}$, the differences in solution quality appear mostly inconsequential. It is also interesting to observe that there are minimal changes in the ideal QPU execution time when using different annealing times for a fixed number of anneal-read cycles. This is due to an implementation detail of the QPU, where reading solutions takes around 100 μs , which dominates the ideal execution times presented in Figure 6 when τ is less than 100 μs . It is also interesting to observe that the wall-clock QPU execution times (i.e., times including service overheads) are much longer than idealized times, typically ranging between two and eight seconds. These wall-clock results further suggest that increasing the annealing time typically has little effect on the overall realized execution time, as most of the time is dominated by the selected number of anneal-read cycles and service overheads.

Given the diminishing solution quality as annealing time increases, as well as marked execution time increases for $\tau = 312.5 \mu\text{s}$, in this work, we adopt an annealing time of $\tau = 62.5 \mu\text{s}$, which strikes a balance between solution quality and execution time. This selection is reflected in Section 3.

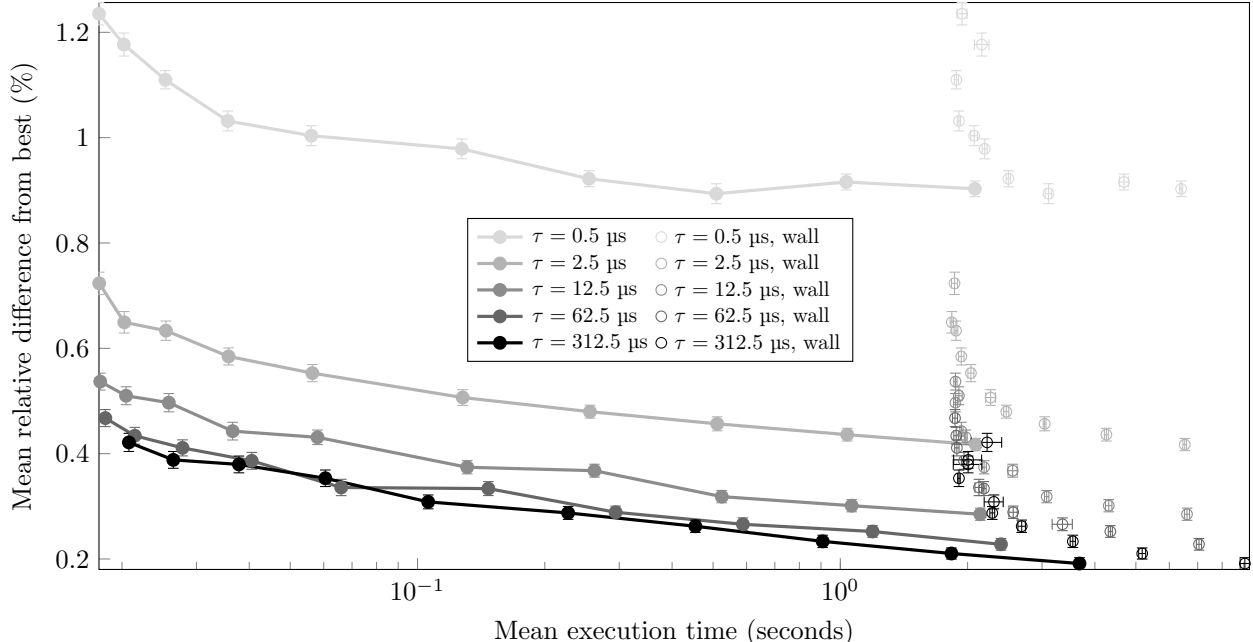


Figure 6: Effects of annealing time on solution quality and ideal/wall-clock execution time for QA hardware, averaged over 50 CBFM-P instances with 5,387 decision variables (PEGASUS lattice size sixteen). Here, each point corresponds to a mean relative difference, computed over 50 individual relative differences from the best solution obtained for each instance. Vertical error bars correspond to the standard error of each mean. Horizontal error bars correspond to standard errors of each mean solve time, each of which is based on a particular QPU execution time parameterization (e.g., 2,560 anneal-read cycles).

D Additional Run Time Analysis

In this section, we expand on the computational results presented in Section 3 by showing the performance results over all of the solution methods considered in this appendix and conducting an average case analysis, accompanying a characteristic example. These additional results serve to motivate the selection of the five methods presented in Section 3, as well as to show that the characteristic example presented in this work is a suitable representative, not an outlier, of the CBFM-P instance class.

To review the computational setting, all of the classical optimization algorithms were executed on a system with two Intel Xeon E5-2695 v4 processors, each with 18 cores at 2.10 GHz, and 125 GB of memory. We present an evaluation of the above optimization techniques on problem instances of the largest CBFM-P Ising models that we considered on the `Advantage.system4.1` system, containing 5,387 variables. For each solution technique, parameters that control the execution time of the algorithm (e.g., number of reads for QA, the number of sweeps in SA, or the wall-clock time limit of an IQP method) were varied per the parameterizations described throughout Appendix B to better understand their effects on solution quality. The plots show the relative difference in the solution quality (to the best-known solution) over the solve time corresponding to a parameterization.

The benchmarking results for all methods on CBFM-P instance “16” (of 50) are illustrated in Figure 7. A summary of these results follows the discussion of Section 3. However, this figure justifies our exclusion of some methods. In particular, we observe that: (1) the CPLEX IQP and GUROBI ILP models are not competitive compared to the GUROBI IQP model and do not bring added insights, and (2) the heuristic methods of tabu search and steepest coordinate descent become stuck in similar local minima, providing limited additional insight. Message passing provides a minimum difference of 162% and does not appear in the plot’s range. It can also be argued that SVMC brings limited additional insight over the SA heuristic. However, we elected to include this in Section 3, given the established history of comparing QA to SVMC in the literature. For heuristic methods, SA and PT-ICM provide the most interesting run time and quality

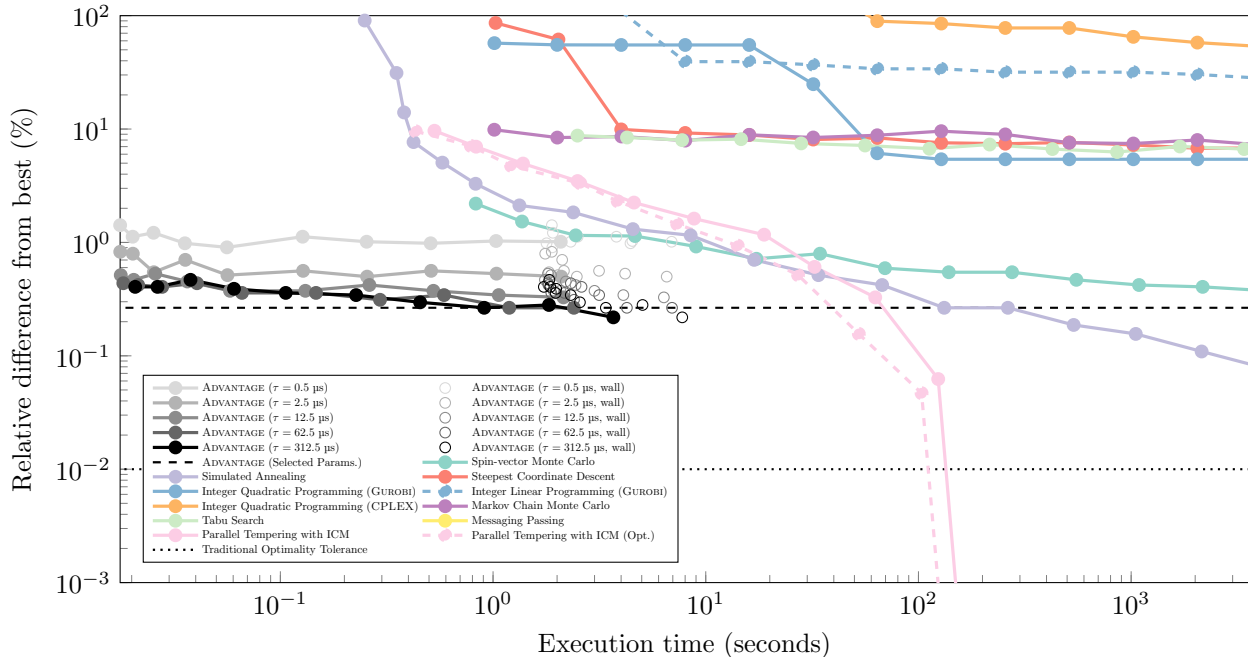


Figure 7: Evaluation of solution quality for a characteristic problem of the CBFM-P instance class with 5,387 decision variables (PEGASUS lattice size sixteen).

tradeoffs and were often the only methods able to match solutions found by the QA hardware. Overall, we made the following selections: steepest coordinate descent for representing a greedy approach, GUROBI IQP for representing an off-the-self complete search approach, SVMC by precedent, and SA and PT-ICM as state-of-the-art alternatives.

Given that CBFM-P defines a distribution of randomly generated optimization instances, it is important to quantify how stable the performance characteristics are across multiple instances from this class. Figure 8 presents such an analysis. It is similar to the other analyses that have been presented but shows performance *averages* across 50 randomly generated instances. Error bars are used to show the standard error across multiple CBFM-P instances, but they tend to be difficult to distinguish, as the variance of results across instances is often small. Message passing again provides a minimum difference of 162% and does not appear in the plot’s range. Overall, these average case results show trends very similar to the characteristic case that is presented in the rest of the paper, providing a strong indication of the stability of the performance characteristics of CBFM-P instances.

D.1 Solution Quality Details

To further elaborate on the consistency of the results presented in Section 3 and support the research community in future benchmarking efforts, Table 1 in this section details the best-known objective values for the 50 largest CBFM-P instances that were considered in this work. These instances consist of 5,387 decision variables and are provided as part of the paper’s supplementary material for future study. In particular, Table 1 reports the *best* objective values found by the representative solution methods of Section 3 and their parameterizations described in and Appendix B. These detailed results further highlight the consistency in the CBFM-P instances at this problem size, as the qualitative behavior of each solution approach is consistent across all of the instances. It is important to also note that this table only provides *best-known* solutions for these fifty problem instances. It was observed that the lower bounds produced by the IQP methods were very weak. Developing tight lower bounds and optimality proofs for these instances remains an important topic for future work.

| Instance | Best Known | QA (Avg. 4.1) | SA | PT-ICM | SVMC | IQP | SCD |
|----------|------------|---------------|----------|----------|----------|----------|----------|
| 1 | -12757.0 | -12723.0 | -12745.0 | -12757.0 | -12717.0 | -12107.0 | -11881.0 |
| 2 | -12803.0 | -12791.0 | -12799.0 | -12803.0 | -12781.0 | -12115.0 | -11923.0 |
| 3 | -12763.0 | -12717.0 | -12745.0 | -12763.0 | -12709.0 | -11933.0 | -11917.0 |
| 4 | -12839.0 | -12819.0 | -12831.0 | -12839.0 | -12803.0 | -12115.0 | -11987.0 |
| 5 | -12730.0 | -12692.0 | -12708.0 | -12730.0 | -12688.0 | -12032.0 | -11862.0 |
| 6 | -12828.0 | -12796.0 | -12810.0 | -12828.0 | -12782.0 | -12024.0 | -11936.0 |
| 7 | -12775.0 | -12739.0 | -12769.0 | -12775.0 | -12723.0 | -12087.0 | -11907.0 |
| 8 | -12892.0 | -12878.0 | -12888.0 | -12892.0 | -12862.0 | -12086.0 | -11988.0 |
| 9 | -12699.0 | -12665.0 | -12679.0 | -12697.0 | -12645.0 | -11977.0 | -11821.0 |
| 10 | -12959.0 | -12933.0 | -12947.0 | -12959.0 | -12929.0 | -12327.0 | -12099.0 |
| 11 | -12756.0 | -12720.0 | -12738.0 | -12756.0 | -12710.0 | -11900.0 | -11858.0 |
| 12 | -12736.0 | -12714.0 | -12722.0 | -12736.0 | -12712.0 | -12110.0 | -11870.0 |
| 13 | -12704.0 | -12666.0 | -12680.0 | -12704.0 | -12670.0 | -11988.0 | -11840.0 |
| 14 | -12828.0 | -12786.0 | -12808.0 | -12828.0 | -12778.0 | -12088.0 | -11924.0 |
| 15 | -12882.0 | -12856.0 | -12878.0 | -12882.0 | -12838.0 | -12208.0 | -11972.0 |
| 16 | -12819.0 | -12785.0 | -12809.0 | -12819.0 | -12771.0 | -12125.0 | -11951.0 |
| 17 | -12851.0 | -12821.0 | -12841.0 | -12851.0 | -12799.0 | -12205.0 | -12025.0 |
| 18 | -12834.0 | -12802.0 | -12818.0 | -12834.0 | -12804.0 | -12214.0 | -11956.0 |
| 19 | -12994.0 | -12936.0 | -12980.0 | -12994.0 | -12936.0 | -12266.0 | -12096.0 |
| 20 | -12712.0 | -12684.0 | -12706.0 | -12712.0 | -12668.0 | -12016.0 | -11852.0 |
| 21 | -12854.0 | -12838.0 | -12844.0 | -12854.0 | -12818.0 | -12096.0 | -11956.0 |
| 22 | -12854.0 | -12840.0 | -12848.0 | -12854.0 | -12834.0 | -12150.0 | -11930.0 |
| 23 | -12825.0 | -12797.0 | -12815.0 | -12825.0 | -12789.0 | -12079.0 | -11989.0 |
| 24 | -12820.0 | -12780.0 | -12802.0 | -12820.0 | -12770.0 | -12056.0 | -11956.0 |
| 25 | -12731.0 | -12703.0 | -12717.0 | -12731.0 | -12695.0 | -12003.0 | -11857.0 |
| 26 | -12869.0 | -12835.0 | -12853.0 | -12869.0 | -12807.0 | -12109.0 | -11993.0 |
| 27 | -12908.0 | -12884.0 | -12900.0 | -12908.0 | -12872.0 | -12126.0 | -12062.0 |
| 28 | -12754.0 | -12714.0 | -12740.0 | -12754.0 | -12710.0 | -11936.0 | -11910.0 |
| 29 | -12768.0 | -12734.0 | -12748.0 | -12768.0 | -12736.0 | -11934.0 | -11890.0 |
| 30 | -12778.0 | -12754.0 | -12772.0 | -12778.0 | -12726.0 | -12026.0 | -11866.0 |
| 31 | -12852.0 | -12830.0 | -12840.0 | -12852.0 | -12826.0 | -12074.0 | -11980.0 |
| 32 | -12857.0 | -12813.0 | -12839.0 | -12857.0 | -12805.0 | -12193.0 | -11973.0 |
| 33 | -12848.0 | -12820.0 | -12834.0 | -12848.0 | -12798.0 | -12040.0 | -11966.0 |
| 34 | -12851.0 | -12825.0 | -12833.0 | -12851.0 | -12819.0 | -12045.0 | -11939.0 |
| 35 | -12870.0 | -12840.0 | -12864.0 | -12870.0 | -12838.0 | -12130.0 | -12020.0 |
| 36 | -12798.0 | -12788.0 | -12794.0 | -12798.0 | -12770.0 | -12158.0 | -11932.0 |
| 37 | -12796.0 | -12758.0 | -12780.0 | -12796.0 | -12750.0 | -12076.0 | -11926.0 |
| 38 | -12883.0 | -12857.0 | -12867.0 | -12883.0 | -12857.0 | -12149.0 | -11999.0 |
| 39 | -12849.0 | -12837.0 | -12841.0 | -12849.0 | -12827.0 | -12217.0 | -12003.0 |
| 40 | -12909.0 | -12899.0 | -12905.0 | -12909.0 | -12895.0 | -12037.0 | -12023.0 |
| 41 | -12829.0 | -12807.0 | -12827.0 | -12829.0 | -12805.0 | -12117.0 | -11925.0 |
| 42 | -12710.0 | -12692.0 | -12700.0 | -12710.0 | -12690.0 | -12036.0 | -11834.0 |
| 43 | -12727.0 | -12699.0 | -12717.0 | -12727.0 | -12681.0 | -11977.0 | -11861.0 |
| 44 | -12863.0 | -12839.0 | -12849.0 | -12863.0 | -12827.0 | -12097.0 | -12013.0 |
| 45 | -12822.0 | -12788.0 | -12814.0 | -12822.0 | -12772.0 | -12166.0 | -11936.0 |
| 46 | -12741.0 | -12721.0 | -12731.0 | -12741.0 | -12719.0 | -11977.0 | -11871.0 |
| 47 | -12830.0 | -12792.0 | -12816.0 | -12830.0 | -12772.0 | -12210.0 | -11988.0 |
| 48 | -12877.0 | -12847.0 | -12873.0 | -12877.0 | -12825.0 | -12137.0 | -11997.0 |
| 49 | -12792.0 | -12774.0 | -12782.0 | -12792.0 | -12756.0 | -12088.0 | -11914.0 |
| 50 | -12806.0 | -12774.0 | -12788.0 | -12806.0 | -12758.0 | -12048.0 | -11982.0 |

Table 1: A summary of the best objective values found among the representative solution methods on the largest instances considered in this work, with 5,387 decision variables (i.e., PEGASUS lattice size sixteen).

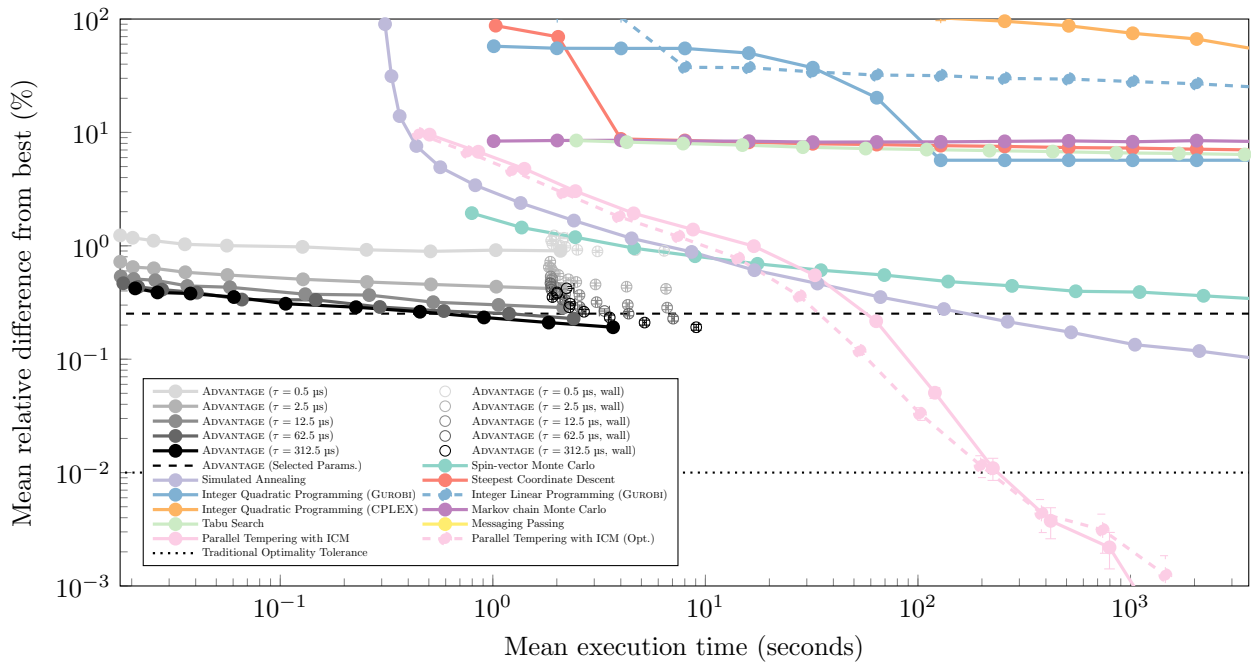


Figure 8: Evaluation of average solution quality over 50 CBFM-P instances with 5,387 decision variables (PEGASUS lattice size sixteen). Each point corresponds to a mean relative difference, computed over 50 individual relative differences from the best solution obtained for each instance. Vertical and horizontal error bars correspond to the standard errors of each mean relative difference and each mean solve time, respectively, but tend to be difficult to distinguish because of their small magnitudes.